Journal of Metals, Materials and Minerals, 37(1), e2799, 2027

Eco-friendly preparation and characterization of avocado waste-derived silver nanoparticles-embedded alginate films for potential wound dressing use

Rasha ABDULBARI[1], Deniz UZUNOĞLU DOĞRUYOL[1,*], and Ayla ÖZER[1]

[1] *Mersin University, Faculty of Engineering, Department of Chemical Engineering, Mersin, Türkiye*

***Corresponding author e-mail**: duzunoglu@mersin.edu.tr

Received date:
29 June 2026
Revised date:
20 September 2026
Accepted date:
14 October 2026

Keywords:
Alginate films;
Avocado peel waste;
Green synthesis;
Silver nanoparticles;
Wound dressing applications

Abstract

The ever-increasing volume of waste generated in the avocado industry poses an environmental problem; however, thanks to the valuable bio-components contained within this waste, this situation presents a potential to be transformed from a problem into an opportunity. In this study, silver nanoparticles (AgNPs) were synthesized using a green method with avocado peel extract as a biogenic reducing and stabilizing agent; the synthesized AgNPs were embedded into sodium alginate (SA) films to obtain functional biomaterials for wound dressing applications. The changes in physicochemical properties (Water resistance, swelling index, gel fraction, degradation behavior, and water vapor transmission rate (WVTR)) of the prepared AgNPs@SA films were investigated by varying the amounts of their components (alginate amount, $AgNO_3$ concentration, and extract concentration). In terms of the obtained physicochemical properties, the film formulation using 2.0 g alginate, 2.0 mM $AgNO_3$, and 0.20 $g \cdot mL^{-1}$ extract was selected as optimum. The film synthesized with the determined optimum formulation was found to have an average thickness of 0.351 mm, a suitable WVTR value, and antibacterial activity against *Staphylococcus aureus* and *Pseudomonas aeruginosa*. Mechanical analysis results show that AgNPs@SA films exhibit a ductile and viscoelastic structure characterized by high elongation and sufficient tensile strength, indicating potential for use as a flexible and stable wound dressing. Characterization studies (SEM, EDX, FTIR, XRD, and XPS) supported the successful green synthesis of AgNPs and provided evidence consistent with their incorporation into the alginate films, while indicating the involvement of plant-derived components in nanoparticle synthesis. The findings indicate that avocado peel waste can be transformed into a value-added product for environmentally friendly wound dressing applications.

1. Introduction

Worldwide avocado (Persea americana) production is approximately 9 million tons per year, while Türkiye's annual production is around 35,000 tons [1]. Avocado is a highly nutritious food and has become a significant agricultural product globally due to its versatile uses. For example, it is used as a valuable source of oil in food and cosmetic applications, while its bioactive compounds make it a raw material in the pharmaceutical and functional food industries. Global population growth, as with many agricultural products, has led to a significant increase in avocado consumption and industrial processing. This increased consumption also leads to the generation of high amounts of by-products such as peel, seed, and pulp residues. Since these wastes constitute approximately 30% to 45% of the total weight of the fruit, they must be disposed of properly [2]. Failure to properly dispose of or improper disposal of avocado processing waste poses a potential for serious environmental and public health problems. Avocado peels, seeds, and pulp, due to their high moisture and organic matter content, can lead to rapid microbial decomposition and consequently bad odors when left in landfills. Uncontrolled decomposition of them easily biodegradable waste can increase greenhouse gas emissions and lead to soil acidification. Nutrients such as nitrogen, phosphorus, and potassium found in avocado waste can leach through precipitation or surface runoff, contaminating nearby water sources and disrupting the balance of aquatic ecosystems [2,3]. Besides, the uncontrolled accumulation of avocado wastes with high moisture content can create suitable breeding grounds for insects and rodents, increasing the risk of infectious disease spread. Particularly in developing regions with inadequate solid waste management, the continuous accumulation of avocado wastes not only increases the environmental burden but can also lead to significant economic opportunity losses due to the underutilization of a potentially valuable biomass resource [4]. Therefore, there is an urgent need for sustainable valorization strategies to reduce the environmental impact of avocado-derived waste and to ensure resource recovery within the framework of a circular bioeconomy approach.

The evaluation of agricultural waste as biogenic reducing and stabilizing agents in the green synthesis of nanomaterials is one of the promising approaches to reduce the environmental impact of such waste. Plant wastes such as fruit peels and seeds are rich in polyphenols, flavonoids, terpenoids, and other phytochemical components that have the ability to reduce metal ions and stabilize the resulting nanoparticles. These properties eliminate the need for toxic chemical reagents, offering an environmentally friendly synthesis process. Accordingly, avocado peels and seeds stand out as abundant and renewable biogenic

resources that can effectively direct nanoparticle formation with its high antioxidant and phenolic compound content [5–8]. This valorization approach enables the conversion of biodegradable wastes into functional nanomaterials, thereby reducing the environmental burden of waste and contributing to an ecologically sustainable and circular bioeconomy-based production model [9].

Among the nanomaterials studied in the literature, silver nanoparticles (AgNPs) have attracted more attention due to their localized surface plasmon resonance [10], high surface reactivity, and strong antimicrobial activity against various microorganisms [11–14]. However, their tendency to aggregate and potential cytotoxic effects can limit their direct use in biomedical applications. To overcome these limitations, nanoparticles can be stabilized, ion release controlled, and biocompatibility increased using biopolymer materials [15].

Sodium alginate (SA) is a natural linear anionic polysaccharide extracted from brown seaweed, which has biodegradable, non-toxic, hydrophilic structure, and superior film-forming properties. Structurally, alginate is composed of β-D-mannuronic (M) and α-L-guluronic (G) acid units, contains abundant hydroxyl and carboxyl groups. These groups are adsorbed onto the surface of metallic nanoparticles, creating electrostatic repulsive forces between the nanoparticles and initially limiting aggregation [16,17].

The embedding of AgNPs into alginate films provides the polymer structure with enhanced mechanical integrity, moisture control, and antimicrobial activity, thus making the polymer structure a suitable, multifunctional nanocomposite material for biomedical and packaging applications [18,19]. The controlled swelling and hydrophilic character of alginate allows for the slow release of silver ions, thus minimizing cytotoxic effects and ensuring long-term antimicrobial efficacy [20]. Furthermore, the high oxygen and water vapor permeability of alginate provides a suitable moist environment for wound healing, which is advantageous for its use as a wound dressing [21]. Numerous studies have reported that the incorporation of AgNPs into alginate-based matrices can significantly improve antibacterial performance while maintaining the favorable biocompatibility of alginate [22–26].

In this context, the incorporation of green synthesized AgNPs into sodium alginate films provides a dual advantage by combining environmentally friendly nanoparticle production with the development of biopolymer-based functional materials. The resulting AgNPs-alginate films offer a sustainable approach to produce next-generation antimicrobial biomaterials by combining the sustainability of green synthesis with the physicochemical strength of polysaccharide matrices.

Although AgNPs-containing alginate-based wound dressing materials and plant-mediated synthesis of AgNPs have been previously reported [6,22–25], the utilization of AgNPs biosynthesized specifically from avocado peel waste in alginate film matrices remains relatively unexplored. The present study addresses this gap by combining avocado peel waste valorization with the development of AgNPs-containing alginate films and systematically investigating the influence of formulation parameters on their physicochemical properties for potential wound dressing applications. The novelty of the present study lies not only in the incorporation of avocado peel-derived AgNPs into alginate films, but also in the systematic evaluation of formulation-dependent physicochemical properties. By investigating the effects of alginate amount, silver precursor concentration, and avocado peel extract concentration on multiple film characteristics, this study provides insights into formulation–property relationships relevant to the development of sustainable materials for potential wound dressing applications.

Based on these considerations, the present study aimed to synthesize AgNPs using an aqueous avocado peel extract as a biogenic reducing and stabilizing agent and to incorporate the synthesized nanoparticles into sodium alginate films for potential wound dressing applications. The physicochemical properties of the developed AgNPs@SA films, such as thickness, water resistance, swelling behavior, mass loss, gel fraction, water vapor permeability rate (WVTR), mechanical strength, and antibacterial performance, were systematically investigated in terms of their suitability for wound dressing applications. In addition, structural and chemical characterization of both AgNPs and AgNPs @SA films was performed using SEM, EDX, FT-IR, XRD, and XPS analyses.

2. Materials and methods

2.1 Materials

Chemicals including Silver nitrate ($AgNO_3$, 99.99%), sodium alginate, Calcium chloride ($CaCl_2$, anhydrous, powder, ≥97%), glycerol (99.0%) were purchased from Sigma-Aldrich Chemicals Ltd., Germany. All the chemicals were used without any further purification.

Waste avocado peels were sourced from various local markets and supermarkets in Mersin, Türkiye, and then processed to prepare the aqueous extract.

2.2 Methods

2.2.1 Preparation of aqueous extract of avocado peel

Waste avocado peels were washed with tap water and then deionized water to remove impurities. Following washing, they were dried in an oven at 70°C for 24 h. The dried peels were then cut into small pieces and ground into a fine powder using a laboratory grinder. Then, the desired amount of dried avocado peel powder (2 g to 50 g) was dispersed in 100 mL of deionized water and heated at 45°C for 30 min. The mixture was then magnetically stirred at 25°C for 5 h to ensure the efficient release of plant-derived phytochemicals into the medium. After that the extract was filtered using Whatman No. 1 filter paper, and stored at 4°C until further use.

2.2.2 Green synthesis of silver nanoparticles (AgNPs)

For this purpose, 85 mL of an aqueous silver nitrate ($AgNO_3$) solution at the desired concentration (0.5 mM, 1.0 mM, 2.0 mM, or 5.0 mM), used as a precursor, was mixed with 15 mL of the prepared aqueous extract at the desired concentration (0.02 $g{\cdot}mL^{-1}$, 0.04 $g{\cdot}mL^{-1}$, 0.10 $g{\cdot}mL^{-1}$, 0.20 $g{\cdot}mL^{-1}$, or 0.50 $g{\cdot}mL^{-1}$), acting as a reducing agent. Then, it was magnetically stirred at room temperature for 60 min. As the reaction progressed, the color of mixture changed from light brown to dark brown, indicating the formation of AgNPs. The resulting colloidal suspension containing AgNPs was stored at 4°C for subsequent characterization studies and film preparation [27]. To determine the concentration of obtained AgNPs under different synthesis conditions, the resulting suspensions (100 mL) were centrifuged at 10000 rpm for

5 min. The collected precipitates were washed five times with deionized water under the same centrifugation conditions, followed by drying at 60°C for 24 h and weighing. The obtained AgNPs concentrations ($mg \cdot L^{-1}$) were calculated by dividing the dry masses by the initial suspension volume.

2.2.3 Preparation of AgNPs-embedded alginate films

For preparation of alginate-based films, the desired amount of sodium alginate (0.5 g, 1.0 g, 2.0 g, or 3.0 g) was dissolved in 100 mL of deionized water and it was magnetically stirred at room temperature for 30 min to obtain a homogeneous alginate solution. In order to impart flexibility, 2.0 mL of glycerol as a plasticizer was added to the alginate solution, and stirring was continued for another 15 min. For the nanoparticle embedding, 50 mL of a pre-synthesized AgNPs suspension was added to the as-prepared solution, and the mixture was magnetically stirred at room temperature for 2 h. The resulting homogeneous dispersion was poured into Petri dishes and dried at 60°C for 24 h. After the drying process, the films were immersed in 200 mL of a 2% (w/v) $CaCl_2$ solution for 10 min for cross-linking process. The obtained films were dried at room temperature for 24 h, then washed with deionized water to remove excess calcium ions, and finally dried again at 45°C for 24 h [28]. The prepared films containing AgNPs were thus designated as AgNPs@SA films.

The effect of film formulation parameters such as the sodium alginate amount (0.5 g, 1.0 g, 2.0 g, and 3.0 g), metal precursor concentration (0.5 mM, 1.0 mM, 2.0 mM, and 5.0 mM), and extract concentration (0.02 $g \cdot mL^{-1}$, 0.04 $g \cdot mL^{-1}$, 0.10 $g \cdot mL^{-1}$, 0.20 $g \cdot mL^{-1}$, and 0.50 $g \cdot mL^{-1}$) on the physicochemical properties of AgNPs@SA films were investigated [29]. Based on the obtained physicochemical results, the formulation exhibiting the most balanced combination of water resistance, swelling behavior, gel fraction, degradation profile, and water vapor transmission characteristics was selected as the optimum formulation. Subsequently, AgNPs@SA films prepared under these optimum conditions were subjected to antibacterial, mechanical, and detailed characterization analyses to evaluate their structural, chemical, and functional properties.

2.2.4 Physicochemical properties of AgNPs@SA films

Water resistance

For evaluation the water resistance of AgNPs@SA films, square samples (3 cm × 3 cm) were cut and dried in an oven at 70°C for 24 h. After cooling to room temperature, the initial dry weight (W_i) of each sample was recorded. Then, the films were immersed in distilled water at room temperature. They were removed from distilled water at predetermined time intervals (2 h, 6 h, 12 h, and 24 h), then gently blotted with filter paper to eliminate surface liquid, and weighed to determine the swollen weight (W_a).

The water absorption capacity (W_A %) was calculated using Equation (1):

$$W_A\ (\%) = (W_a - W_i) / W_i \times 100 \quad (1)$$

After that, the films were re-dried in an oven at 70°C for 24 h and the dry weight (Ws) was noted. The water solubility (W_S %) was determined using Equation (2):

$$W_S\ (\%) = (W_i - W_s) / W_i \times 100 \quad (2)$$

These tests simulate the behavior of the films in a moist environment, providing valuable information about their stability, durability, and potential service life when used as wound dressing materials.

Swelling index

The swelling index values were calculated for the evaluation of the liquid absorption capacity. For this aim, square film samples (1 cm × 1 cm) were cut and dried in an oven at 37°C for 6 h. Then, the initial dry weight (W_o) of each sample was recorded. The dried films were immersed in a phosphate-buffered saline (PBS, pH = 7.4) solution at 37°C to simulate physiological conditions and maintained for 24 h.

At the end of the immersion period, the samples were removed from the PBS solution, and excess surface liquid was gently blotted using filter paper. Lastly, the swollen weight (W_s) was recorded and the swelling index (S.I. %) was calculated using Equation (3) [30] :

$$S.I.\ (\%) = (W_s / W_o) \times 100 \quad (3)$$

This test provides an indication of the films' ability to absorb and retain fluids under physiological conditions, which is a critical parameter for evaluating their potential as wound dressing materials.

Weight loss

Square film samples (2 cm × 2 cm) were cut and their initial dry weight (W_o) was recorded. Then, they were immersed in PBS (pH 7.4) solution at 37°C for 14 days. The PBS solution was replaced daily to ensure the complete removal of degraded or dissolved fragments. The samples were removed from the solution at predetermined time intervals (1 day, 2 day, 3 day, 7 day, and 14 day) and dried in an oven at 37°C for 6 h to obtain the final dry weight (W_f).

The weight loss percentage (W.I. %) was calculated using Equation (4) [30] :

$$W.I.\ (\%) = (\ (W_o - W_f) / W_o\ ) \times 100 \quad (4)$$

This test provides insight into the biodegradation profile of the films, reflecting their potential lifetime and stability during the wound-healing process. Controlled degradation behavior is desirable, as it allows the dressing to gradually disintegrate as the wound heals or to sustain drug release over an extended period.

Gel fraction

Square film samples (1 cm × 1 cm) were cut and dried in an oven at 37°C for 6 h. Then, the initial dry weight (W_o) of each film was noted. They were immersed in distilled water and maintained at room temperature for 24 h. Lastly, the films were re-dried in an oven at 37°C for 6 h, and the final dry weight (W_d) was measured.

The gel fraction (GF %) was calculated using Equation (5) [30] :

$$GF\ (\%) = (W_d / W_o) \times 100 \quad (5)$$

The gel fraction indicates the degree of crosslinking within the alginate matrix, reflecting the stability and integrity of the water-

insoluble network structure. A higher gel fraction value corresponds to a more efficient crosslinking process and a stronger three-dimensional polymer network.

Water vapor transmission rate (WVTR)

The water vapor transmission rate (WVTR) of the prepared films was determined according to the ASTM E96-93 (ASTM, 1993) standard method. Accordingly, glass tubes with a diameter of 1.0 cm and a depth of 16 cm were filled with 3.0 g of anhydrous $CaCl_2$, which had been previously dried at 200°C for 1 h to ensure complete dehydration. Then, the openings of the tubes were tightly sealed with the film samples, ensuring an airtight barrier between the tube and the surrounding air. The initial weight of each tube was recorded, and they were placed under ambient conditions.

The samples were weighed at 24 h intervals until a constant weight was reached, indicating equilibrium moisture uptake. The WVTR was calculated in $g \cdot m^{-2} \cdot day^{-1}$ using Equation (6):

$$WVTR = \Delta m / (A \times t) \quad (6)$$

where Δm represents the mass increase (moisture gain) (g) due to water vapor permeation, A is the exposed film surface area (m^2), and t is the exposure time (days).

This measurement provides insight into the films' ability to regulate vapor diffusion across the wound surface, offering valuable information about their suitability for maintaining an optimal healing environment [30].

Film thickness

Film thickness is a critical parameter affecting mechanical strength, gas permeability, and the wound-healing performance. So, thickness values of the optimized film were measured using a digital caliper at five different points, and the mean value was calculated.

Antibacterial activity

The antibacterial activity of the optimized film was evaluated using the disk diffusion method against both a Gram-negative bacterium, *Pseudomonas aeruginosa* (ATCC 27853), and a Gram-positive bacterium, *Staphylococcus aureus* (ATCC 25923). Briefly, sterile circular film samples were prepared under aseptic conditions and placed onto agar plates previously inoculated with the bacterial cultures. Following incubation under suitable growth conditions, the diameters of the inhibition zones were measured using a digital caliper. The antibacterial assays were performed in three independent experiments (n = 3), and the inhibition zone diameters were expressed as mean ± standard deviation (SD).

Mechanical strength

The mechanical behavior of optimized film was evaluated using Dynamic Mechanical Analysis (DMA, TA Instruments Q800) under stress–strain mode at room temperature to assess their viscoelastic and tensile properties.

2.2.5 Characterization studies

AgNPs synthesized using 2.0 mM $AgNO_3$ and 0.02 $g \cdot mL^{-1}$ avocado peel extract were characterized via Scanning electron microscopy (SEM, FEI Quanta 650 Field Emission) for observation of morphology, size distribution, and aggregation behavior; energy Dispersive X-ray Spectroscopy (EDX, integrated with FEI Quanta 650) for the elemental composition; X-ray photoelectron spectroscopy (XPS, Thermo scientific K-Alpha, Monochromatic Al Kα source, 400 µm spot size) for the determination of the chemical composition and oxidation states of the nanoparticles.

The structural and mechanical integrity of the optimized AgNPs @SA films were evaluated by the characterization techniques. Accordingly, SEM-EDX analyses were performed to evaluate surface morphology and AgNPs distribution in the alginate matrix. Fourier transform infrared spectroscopy (FT-IR, Perkin Elmer, 400 cm^{-1} to 4000 cm^{-1}, KBr pellet method) was used to observe functional groups. X-ray Diffraction (XRD, PANalytical EMPYREAN, Cu Kα, λ = 1.54 Å) analysis was carried out for the determination of the crystalline structure of the embedded nanoparticles.

3. Results and discussions

In this study, AgNPs@SA films were prepared by varying the formulation parameters. Accordingly, different amounts of sodium alginate (0.5 g, 1.0 g, 2.0 g, and 3.0 g per 100 mL of deionized water) were used to obtain the polymer matrix. The aqueous extracts of avocado peel powder were utilized as biogenic reducing agents at concentrations ranging from 0.02 $g \cdot mL^{-1}$ to 0.50 $g \cdot mL^{-1}$, while silver nitrate ($AgNO_3$) solutions of 0.5 mM, 1.0 mM, 2.0 mM, and 5.0 mM were used as metal precursors for AgNPs embedding.

The concentrations of obtained AgNPs were determined under different synthesis conditions. At a fixed avocado peel extract concentration of 0.20 $g \cdot mL^{-1}$, increasing the $AgNO_3$ concentration from 0.5 mM to 1.0 mM, 2.0 mM, and 5.0 mM resulted in obtained AgNPs concentrations of 39 $mg \cdot L^{-1}$, 82 $mg \cdot L^{-1}$, 165 $mg \cdot L^{-1}$, and 421 $mg \cdot L^{-1}$, respectively. Similarly, at a constant $AgNO_3$ concentration of 2.0 mM, extract concentrations of 0.02 $g \cdot mL^{-1}$, 0.04 $g \cdot mL^{-1}$, 0.10 $g \cdot mL^{-1}$, 0.20 $g \cdot mL^{-1}$, and 0.50 $g \cdot mL^{-1}$ yielded AgNPs concentrations of 27 $mg \cdot L^{-1}$, 35 $mg \cdot L^{-1}$, 82 $mg \cdot L^{-1}$, 165 $mg \cdot L^{-1}$, and 174 $mg \cdot L^{-1}$, respectively. These results indicate that both $AgNO_3$ and avocado peel extract concentrations influenced the concentration of obtained AgNPs. Notably, the increase in obtained AgNPs concentration became less pronounced above an extract concentration of 0.20 $g \cdot mL^{-1}$, suggesting a diminishing effect of further extract addition under the investigated conditions.

3.1 Physicochemical properties of AgNPs@SA films

3.1.1 Water resistance

In this section, the water absorption (W_A%) and water solubility (W_S%) of AgNPs@SA films were evaluated to determine their resistance to moisture and structural stability in aqueous environments.

The effect of alginate amount on W_A % and W_S % of AgNPs@SA films was illustrated in Figure 1(a–b), respectively. Accordingly, the increase in alginate amount led to a noticeable decrease in both W_A% and W_S%, indicating enhanced structural integrity and water resistance. In addition, a time-dependent increase in W_A% was observed for all

samples, with a more obvious rise at lower alginate contents. This behavior suggests that films with lower polymer content allow faster water diffusion and greater fluid uptake over time. In contrast, films containing higher alginate amounts exhibited a more limited increase in W_A% with immersion time, indicating a more stable and compact structure. In this case, it is thought that higher alginate concentrations led to the formation of more tightly cross-linked polymeric network, thereby restricting water diffusion and polymer chain mobility. The increasing the amount of alginate resulting in an increase in hydrogen bonds between alginate chains provided to the compact structure, which in turn effectively reduced the availability of hydrophilic regions for water interaction [31].

The changes of W_A% and W_S% with $AgNO_3$ concentrations were presented in Figure 2(a–b), respectively. Both of W_A% and W_S% values decreased with the increase in the $AgNO_3$ concentration from 0.5 mM to 5.0 mM, suggesting enhanced compactness and reduced hydrophilicity of the films. As shown in Figure 2(a), W_A% values increased with immersion time for all samples, showing a rapid initial uptake followed by a more gradual increase. This behavior is characteristic of diffusion-controlled swelling, while the overall time-dependent trends remained similar across different $AgNO_3$ concentrations. Based on the inference drawn from Figure 2(b), the higher precursor concentrations led to a denser dispersion of AgNPs within the alginate network, restricting water diffusion and limiting polymer chain relaxation. Consequently, films synthesized with higher $AgNO_3$ concentrations exhibited lower moisture uptake and dissolution, confirming that increased nanoparticle loading reinforces network stability and improved overall water resistance [32].

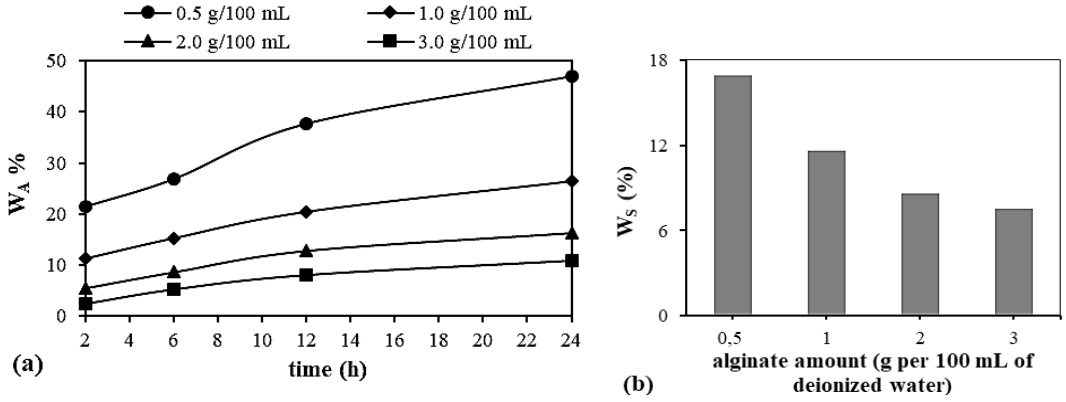


Figure 1. Effect of alginate amount on (a) W_A %, and (b) W_S % of AgNPs@SA films.

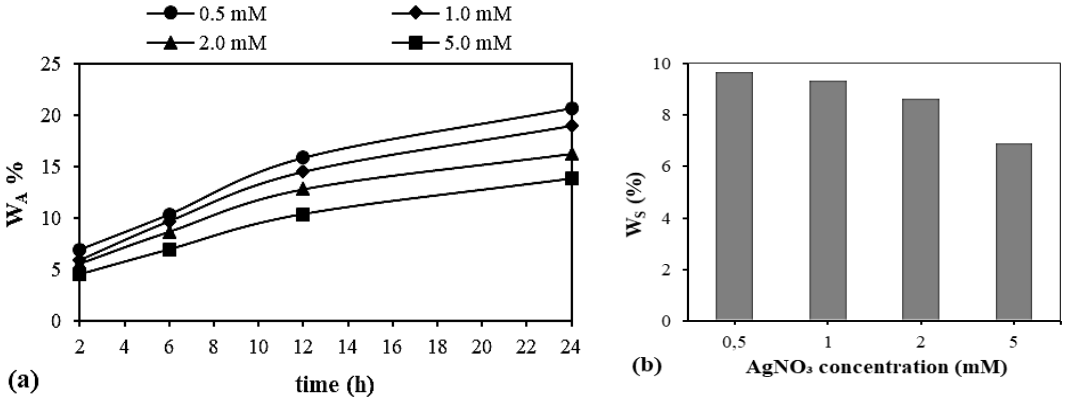


Figure 2. Effect of $AgNO_3$ concentration on (a) W_A %, and (b) W_S % of AgNPs@SA films.

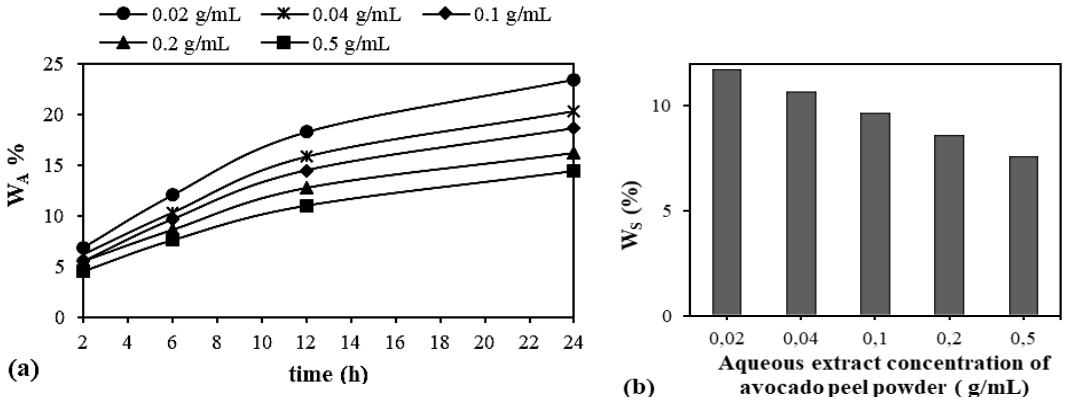


Figure 3. Effect of aqueous extract concentration of avocado peel powder on (a) W_A%, and (b) W_S% of AgNPs@SA films.

The effect of the aqueous extract concentration of avocado peel powder on W_A% and W_S% values was illustrated in Figure 3(a–b), respectively. Both of W_A% and W_S% values decreased with increasing extract concentration from 0.02 g·mL^{-1} to 0.50 g·mL^{-1}, indicating improved compactness and reduced hydrophilicity of the film matrix. W_A% values increased with immersion time for all samples, with the most significant increase observed between 2 h and 12 h, followed by a more moderate rise at longer immersion times. Moreover, the reduction in W_A% with increasing extract concentration became more pronounced at longer immersion times, indicating a stronger resistance to water uptake in films with higher extract content. In this case, the presence of higher extract concentrations promoted the incorporation of more phytochemical compounds—such as phenolics, flavonoids, and reducing sugars—which can form additional hydrogen bonds with alginate chains and enhanced network cohesion. Consequently, the denser structure limited water diffusion and dissolution within the polymer network [31].

Consequently, the water resistance of AgNPs@SA films was strongly dependent on formulation composition. Increasing alginate and $AgNO_3$ concentrations produced more cross-linked networks that restricted water diffusion, while higher aqueous extract of avocado peel powder concentration introduced additional hydrogen bonding sites that reinforced matrix integrity.

3.1.2 Swelling index

The swelling index (S.I.) is a critical factor of a film's ability to retain moisture and maintain stability under physiological conditions, which is particularly important for wound dressing applications. As shown in Figure 4(a–c), all formulation parameters—alginate amount, $AgNO_3$ concentration, and aqueous extract of avocado peel powder concentration—had a notable effect on the swelling behavior of AgNPs@SA films. Increasing alginate amount resulted in a more compact and cross-linked polymer network, thereby restricting water diffusion and reducing S.I. (%). Similarly, higher $AgNO_3$ concentrations enhanced nanoparticle distribution and physical cross-linking within the alginate matrix, leading to lower fluid uptake [28]. Additionally, higher concentrations of aqueous avocado peel powder extract, rich in phenolic and fibrous compounds, contributed to reduced porosity and limited water penetration by reinforcing the polymeric structure [33]. These findings demonstrated that optimized polymer–nanoparticle–extract interactions improved structural stability and moisture regulation, which are important for controlled hydration and the prevention of excessive swelling in biomedical applications.

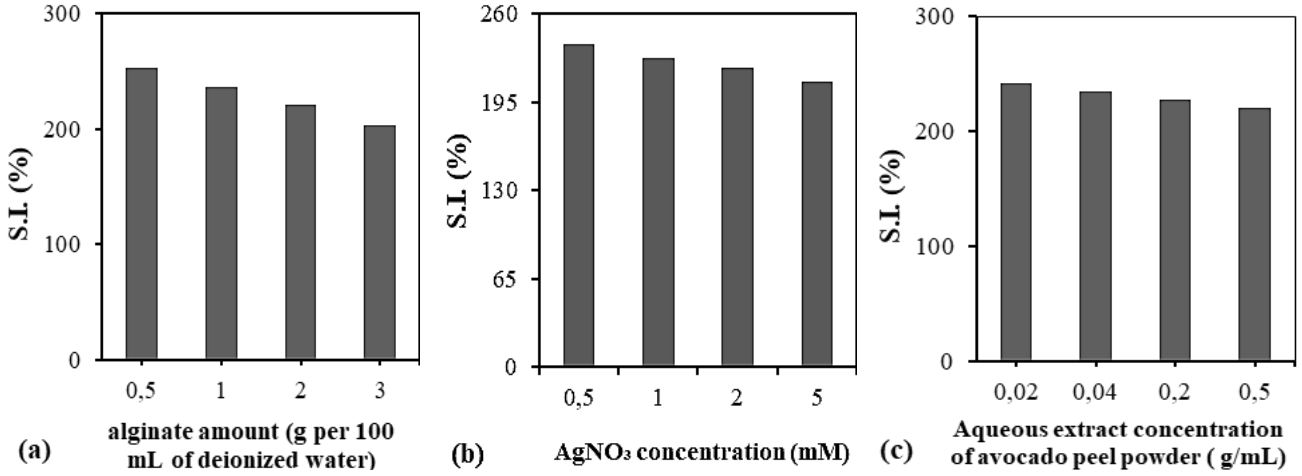


Figure 4. Effect of (a) alginate amount, (b) $AgNO_3$ concentration, and (c) aqueous extract concentration of avocado peel powder on S.I. (%) of AgNPs@SA films.

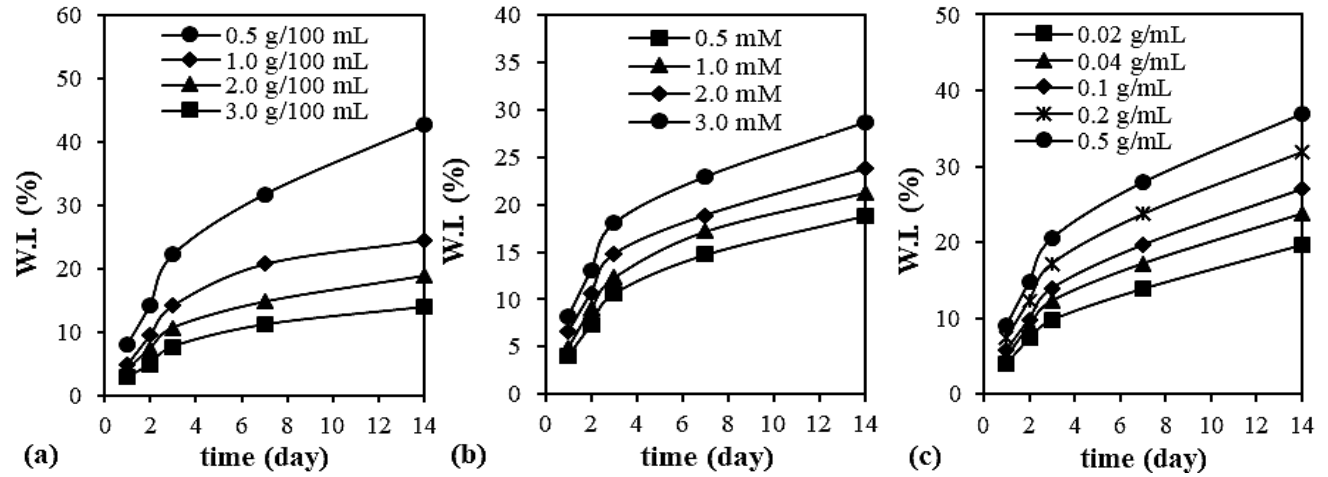


Figure 5. Effect of (a) alginate amount, (b) $AgNO_3$ concentration, and (c) aqueous extract concentration of avocado peel powder on W.I. (%) of AgNPs@SA films.

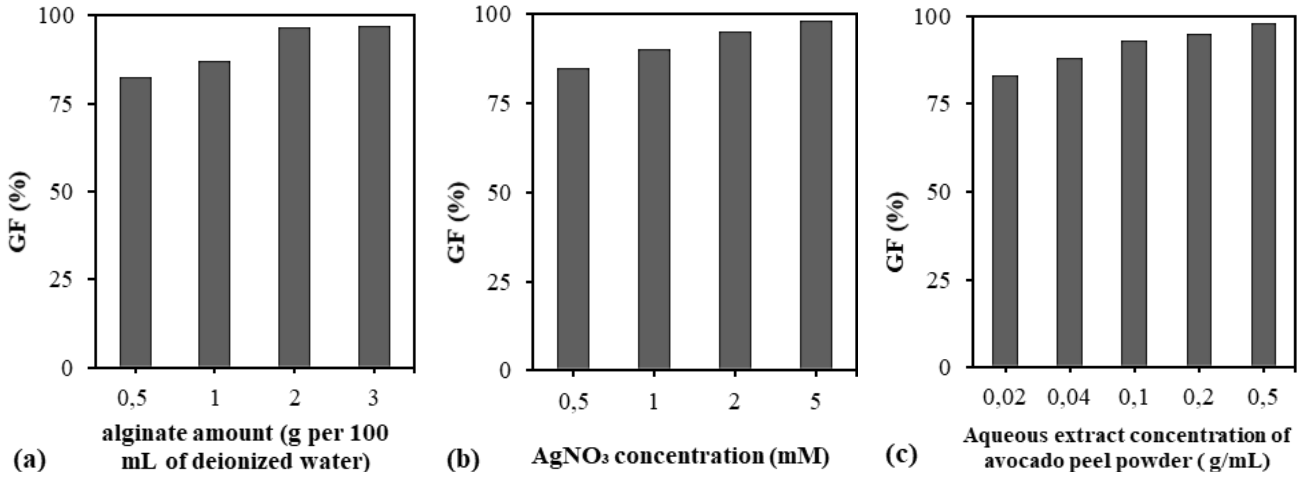


Figure 6. Effect of (a) alginate amount, (b) $AgNO_3$ concentration, and (c) aqueous extract concentration of avocado peel powder on GF (%) of AgNPs@SA films.

3.1.3 Weight loss

The evaluation of weight loss (W.I.) provides valuable insight into the degradation behavior and long-term stability of polymer-based films when exposed to physiological environments. As expected, W.I. (%) values increased progressively with immersion time for all samples, reflecting the gradual hydrolytic degradation of the polymer network. As seen in Figure 5(a–c), the degradation behavior of AgNPs @SA films varied remarkably with changes in alginate amount, $AgNO_3$ concentration, and aqueous extract concentration of avocado peel powder. Films containing more alginate exhibited lower W.I. values, suggesting that more cross-linked network structure limited water diffusion and slowed degradation [34]. This effect became more evident at longer immersion times, where films with lower alginate content showed a more pronounced increase in weight loss. On the contrary, increasing $AgNO_3$ concentration led to a gradual rise in weight loss, likely due to the formation of small voids and weaker bonding between AgNPs and the alginate matrix [32]. A similar time-dependent increase was observed for all $AgNO_3$ concentrations, with slightly higher degradation levels maintained throughout the entire immersion period at elevated precursor concentrations. A similar situation was noticed for higher avocado peel extract concentrations, where phenolic compounds and fibrous residues disrupted the compact polymer structure, making it more prone to hydrolytic breakdown. Accordingly, films with higher extract content exhibited greater weight loss over time, particularly at extended immersion durations. These results indicated that while higher alginate content enhanced stability, excessive $AgNO_3$ or extract addition can disturb the matrix structure and accelerate film degradation.

3.1.4 Gel fraction

Gel fraction (GF %) analysis is an important value of the structural integrity and crosslinking efficiency of polymeric films after exposure to water. As shown in Figure 6 (a–c), the GF (%) of AgNPs@SA films increased consistently with increase in alginate amount, $AgNO_3$ concentration, and aqueous extract concentration of avocado peel powder. Films containing more alginate exhibited a denser and more stable network, which limited dissolution and confirmed strong crosslinking between alginate chains. Similarly, increasing $AgNO_3$ concentration enhanced GF (%), suggesting that the formation of AgNPs contributed to additional coordination and electrostatic interactions within the matrix, improving its mechanical and water-resistant stability [32]. The addition of avocado peel extract also positively affected GF (%), likely due to the presence of phenolic and flavonoid compounds capable of forming hydrogen bonds with alginate molecules, further strengthening the polymeric network [31]. These findings indicated that higher alginate, $AgNO_3$, and extract concentrations promoted stronger crosslinked structures, which enhanced the durability and insolubility of AgNPs@SA films in aqueous environments.

3.1.5 Water vapor transmission rate (WVTR)

Water vapor transmission rate (WVTR) and moisture gain are critical parameters for evaluating the suitability of wound dressing materials, as they directly influence the balance between moisture retention and exudate removal. As shown in Figure 7(a–c), the WVTR and moisture gain of AgNPs@SA films decreased consistently with increasing alginate amount, $AgNO_3$ concentration, and avocado peel extract content. This trend indicated that higher solid and nanoparticle loadings contributed to a denser and less porous film matrix, effectively restricting vapor diffusion [35,36].

Films with greater alginate content exhibited reduced WVTR values due to increased viscosity and compact polymer packing, which limited the permeability of water vapor through the matrix. Similarly, higher $AgNO_3$ concentrations enhanced the formation of AgNPs, which acted as additional physical crosslinkers, strengthening the network and reducing void spaces that facilitated vapor passage. The incorporation of avocado peel extract also led to a decrease in WVTR, likely owing to the phenolic and tannin compounds that interacted with alginate chains, reducing hydrophilic pore sites and tightening the film structure [37].

In summary, the physicochemical and functional evaluations collectively demonstrated that the AgNPs@SA films possessed desirable properties for wound dressing applications. Increasing alginate content consistently enhanced structural integrity, reduced water uptake, and improved moisture control due to the formation of a denser and more cross-linked network. Moderate $AgNO_3$ concentrations further reinforced this structure by promoting AgNPs formation, which acted as additional crosslinkers; however, excessive nanoparticle loading slightly accelerated

degradation through microstructural irregularities. The incorporation of aqueous avocado peel extract contributed additional hydrogen bonding sites and bioactive phenolic compounds, improving compactness and water resistance while maintaining biodegradability. Accordingly, the formulation selection was based on a comparative assessment of the physicochemical properties presented in Figure 1–7, rather than the maximization or minimization of an individual parameter. The balance between water resistance, swelling behavior, structural stability, weight loss, and WVTR was considered the primary criterion for identifying the most appropriate formulation.

Considering the combined effects of alginate amount, $AgNO_3$ content, and aqueous extract of avocado peel, the composition containing 2.0 g alginate amount, 2.0 mM $AgNO_3$, and 0.20 $g \cdot mL^{-1}$ aqueous extract concentration was determined to be the most rational and balanced formulation. At lower alginate amounts, the films exhibited greater water uptake and weight loss, whereas higher alginate amounts further restricted swelling and water vapor transmission. As shown in Figure 6(a), increasing the alginate amount from 2.0 g to 3.0 g resulted in only a slight increase in gel fraction (approximately 96% to 97%), while the swelling index decreased from approximately 220% to 200% (Figure 4(a)). Therefore, 2.0 g alginate was preferred to maintain a relatively high gel fraction without unnecessarily restricting fluid uptake. Similarly, a moderate $AgNO_3$ concentration of 2.0 mM provided a suitable balance between film stability and moisture transport. Increasing the $AgNO_3$ concentration from 2.0 mM to 5.0 mM resulted in a relatively small increase in gel fraction (approximately 95% to 98%; Figure 6(b)), accompanied by a decrease in WVTR from approximately 2200 $g \cdot m^{-2} \cdot day^{-1}$ to 2050 $g \cdot m^{-2} \cdot day^{-1}$ (Figure 7(b)). Thus, 2.0 mM was selected to maintain the desired physicochemical balance without using the highest investigated precursor concentration. The avocado peel extract concentration of 0.20 $g \cdot mL^{-1}$ was selected by considering its effects on water resistance, gel fraction, weight loss, and WVTR. Furthermore, increasing the extract concentration from 0.20 $g \cdot mL^{-1}$ to 0.50 $g \cdot mL^{-1}$ resulted in only a slight increase in the concentration of obtained AgNPs, from 165 $mg \cdot L^{-1}$ to 174 $mg \cdot L^{-1}$ (approximately 5.5%), while the 14 day weight loss increased from approximately 32% to 37% (Figure 5(c)). These findings supported the selection of 0.20 $g \cdot mL^{-1}$ as a more balanced extract concentration.

It should be noted that the selected formulation represents the most balanced composition within the investigated experimental range, based on comparative physicochemical screening rather than a formal mathematical optimization procedure. Therefore, this specific combination offered the best compromise between water resistance, swelling control, weight loss, biodegradability, and vapor permeability, making it the most appropriate condition for the synthesis of AgNPs@SA films intended for wound dressing applications. At this formulation, the film thickness was measured, antibacterial activity tests and mechanical strength analysis were conducted to assess its functional performance. In addition, all structural characterization analyses were performed using films prepared under these optimized conditions, providing a comprehensive understanding of the morphological and chemical properties of the AgNPs@SA films.

3.1.6 Film thickness

The average thickness of the AgNPs@SA films was measured to be 0.351 mm. Film thickness is a critical parameter that directly affects the moisture retention capacity, oxygen permeability, and mechanical strength of wound dressing materials. According to the literature, optimal wound dressing thickness typically ranges between 0.20 mm and 0.50 mm, which ensures sufficient gas exchange while maintaining an effective barrier against microbial penetration [38,39]. Within this context, the thickness value obtained for the AgNPs@SA films fell within the ideal range, indicating that the films possessed suitable physical characteristics for potential wound dressing applications.

3.1.7 Antibacterial activity

The optimized AgNPs@SA film containing 2.0 g of alginate, 2.0 mM $AgNO_3$, and 0.2 $g \cdot mL^{-1}$ aqueous avocado peel extract exhibited clear antibacterial activity against both *Staphylococcus aureus* (Gram-positive) and *Pseudomonas aeruginosa* (Gram-negative). Inhibition zone diameters of 11 ± 0.58 mm for *S. aureus* and 9 ± 0.69 mm for *P. aeruginosa* were recorded, indicating a more pronounced effect against the Gram-positive strain (Figure 8). Both Gram-positive and

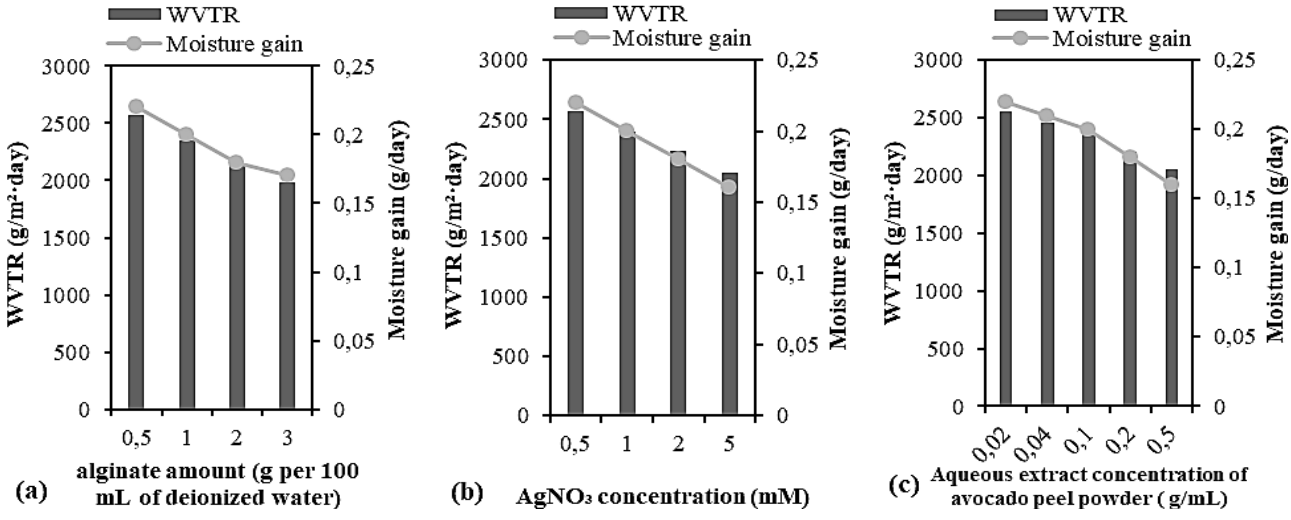


Figure 7. Effect of (a) alginate amount, (b) $AgNO_3$ concentration, and (c) aqueous extract concentration of avocado peel powder on WVTR and moisture gain of AgNPs@SA films.

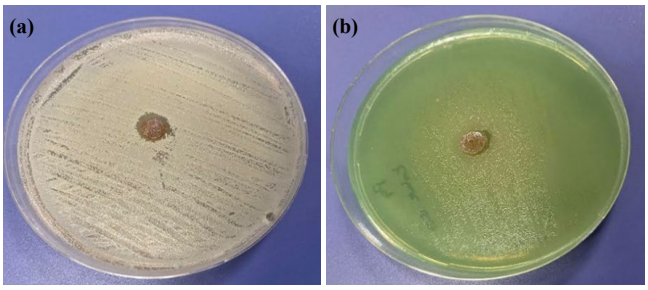


Figure 8. Antibacterial activity of optimized AgNPs@SA film against (a) *S. aureus*, and (b) *P. aeruginosa.*

Gram-negative strains were inhibited, with a slightly higher activity observed against *S. aureus*. Consequently, the AgNPs@SA films demonstrated broad-spectrum antibacterial activity, confirming that the synergistic combination of alginate matrix, silver nanoparticles, and phytochemical-rich avocado peel extract enhanced bactericidal performance. Similar antibacterial behavior of AgNPs-containing alginate-based wound dressing materials has been reported previously, where silver nanoparticles were shown to inhibit both Gram-positive and Gram-negative bacteria through membrane disruption and oxidative stress mechanisms [22–24,26]. These findings supported the potential application of the developed films as bioactive wound dressings capable of preventing infection and promoting a controlled healing environment.

3.1.8 Mechanical strength

The mechanical properties of the AgNPs@SA films exhibited an appropriate balance between elasticity and strength, which is important for their biomedical application. As illustrated in Figure 9 (a–b), the relaxation modulus and stiffness (Figure 9(a)) showed that the viscoelastic response of the film was independent in a wide range of applied load, indicating that its internal network was stable and had uniform energy dissipating ability. It was also inferred from the figures that the stress–strain response (Figure 9(b)) had a characteristic J-curve shape where the stress rose sharply at low strains followed by a more gradual increase with deformation. This behavior was indicative of a ductile and viscoelastic character of the alginate/AgNPs matrix in which conformal polymer chain alignment and internal structural reconfigurations control tensile deformation. The high elongation at break (69.74%) as well as the moderate tensile strength (1.07 MPa) showed that the film can resist large stresses while remaining resistant to failure [40]. In summary, the results demonstrated that the AgNPs@SA film had good flexibility, resilience, and conformability suitable as a wound dressing in terms of mechanical integrity and patient comfort for application.

3.2 Characterization studies

The XPS survey spectrum (Figure 10(a)) confirmed the elemental composition of the biosynthesized AgNPs, showing dominant signals for Ag, O, and C, accompanied by a minor N contribution. The high-resolution Ag 3d spectrum (Figure 10(b)) exhibited a well-defined doublet consistent with metallic silver (Ag^0), with Ag $3d_{5/2}$ located near ~368 eV and Ag $3d_{3/2}$ around ~374 eV, presenting a spin–orbit splitting of approximately 6.0 eV, as typically reported for zero-valent AgNPs. The high-resolution XPS spectrum of C 1s (Figure 10(c)) was deconvoluted into three distinct peaks, which can be assigned to C–C/C–H (285.6 eV), C–O (286.8 eV), and C=O (287.8 eV), indicating the presence of surface-bound organic functional groups that originated from the extract and acted as natural stabilizing agents for the green-synthesized AgNPs. The binding energy observed at 532.28 eV in the O 1s region (Figure 10(d)) corresponded to Ag–O bonding on the nanoparticle surface. This suggested that oxygen-containing biomolecules from the extract interact with silver atoms, leading to the formation of stable Ag–O linkages. The high-resolution N 1s spectrum (Figure 10(e)), recorded within the 393 eV to 410 eV range, revealed two prominent peaks at 399.28 eV and 406.78 eV. The peak at ~399 eV was typically attributed to nitrogen species such as N–H, $–NH_2$, or amide (N–C=O) groups, while the higher-energy peak near 407 eV corresponded to oxidized or protonated nitrogen species. These signals indicated that nitrogen-containing biomolecules from the plant extract were bound to the nanoparticle surface, providing natural capping and stabilization of the green-synthesized AgNPs [41–44].

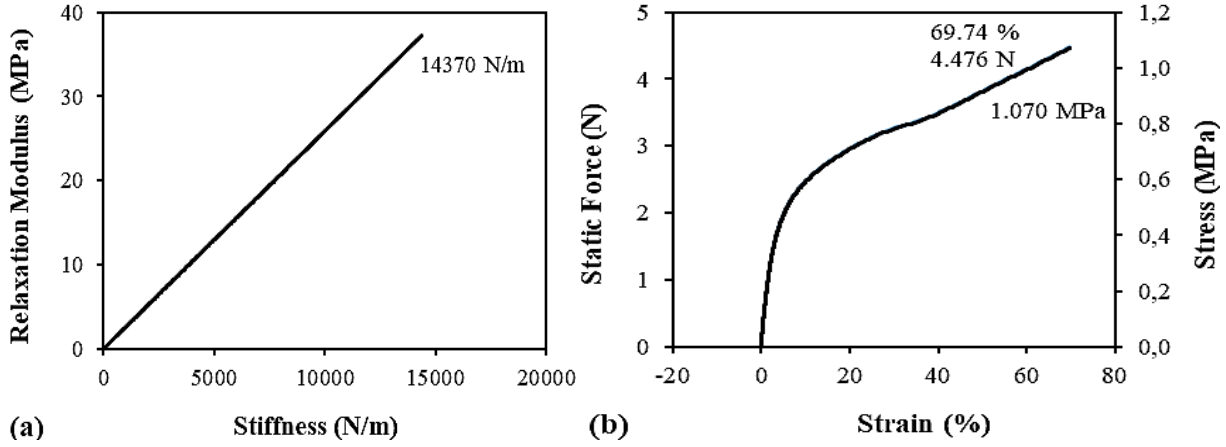


Figure 9. (a) Relationship between relaxation modulus and stiffness, and (b) Stress–strain curve showing the static force and stress variation of optimized AgNPs@SA film.

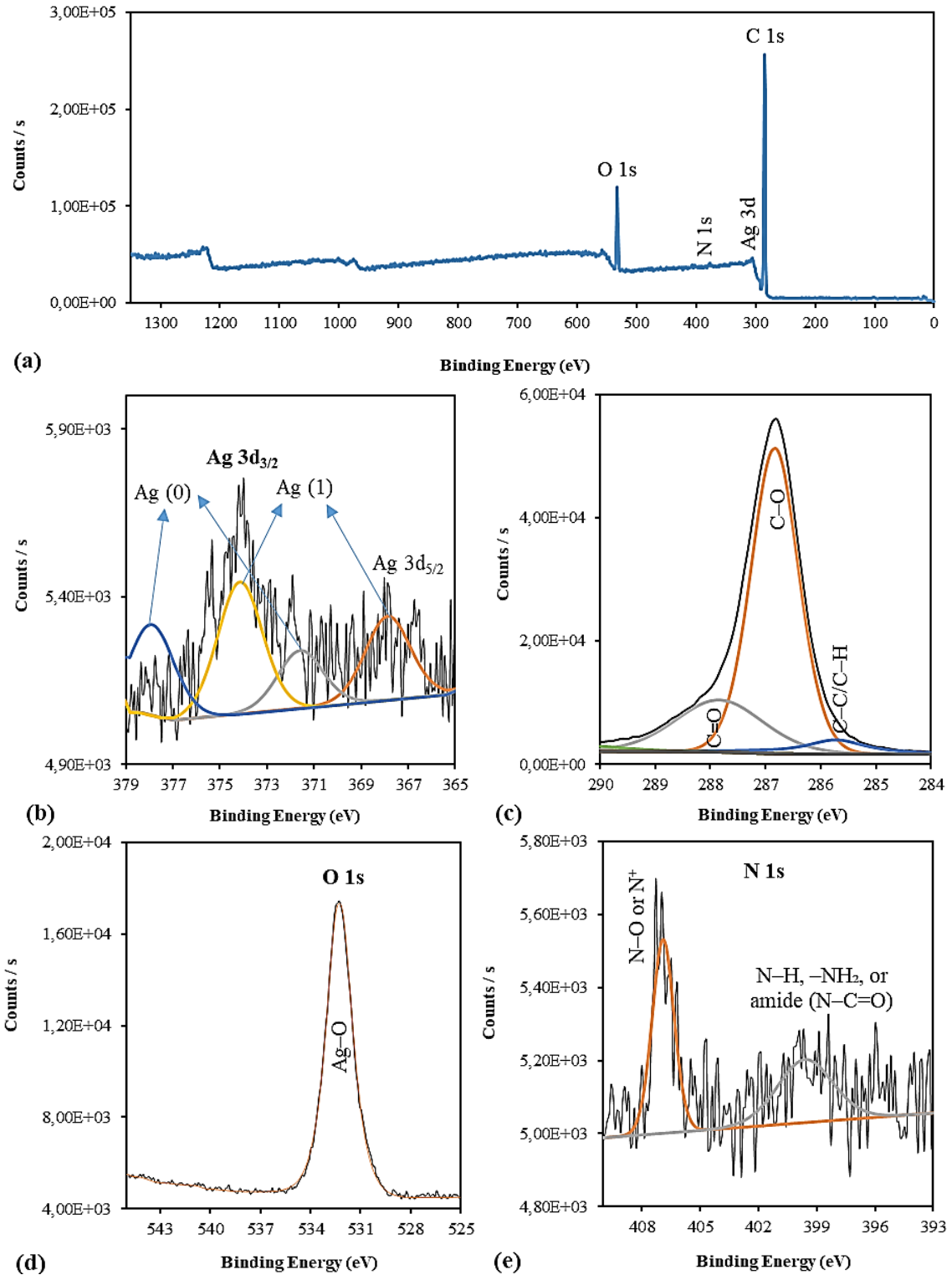


Figure 10. (a) XPS survey spectrum, deconvoluted XPS spectra of (b) Ag 3d, (c) C 1s, (d) O 1s, and (e) N 1s of Ag NPs.

The SEM image shown in Figure 11(a) demonstrated that the green-synthesized AgNPs were mostly spherical and tended to cluster together, forming larger aggregates. Consistent with the SEM observations, the particle size distribution shown in Figure 11(b) indicated a dominant population between ~30 nm to 50 nm, with an average diameter of approximately 49.8 nm (for particles below 100 nm). The appearance of relatively larger particles in the histogram likely resulted not from primary particle growth but from the coalescence or aggregation of smaller nanoparticles, which came into close contact during green synthesis. Such aggregation-driven enlargement is common in biologically mediated nanoparticle synthesis and reflects the interplay between rapid nucleation and partial stabilization by organic capping species. In conclusion, both the SEM morphology and the size distribution supported the successful formation of small AgNPs with some larger aggregates formed by particle clustering.

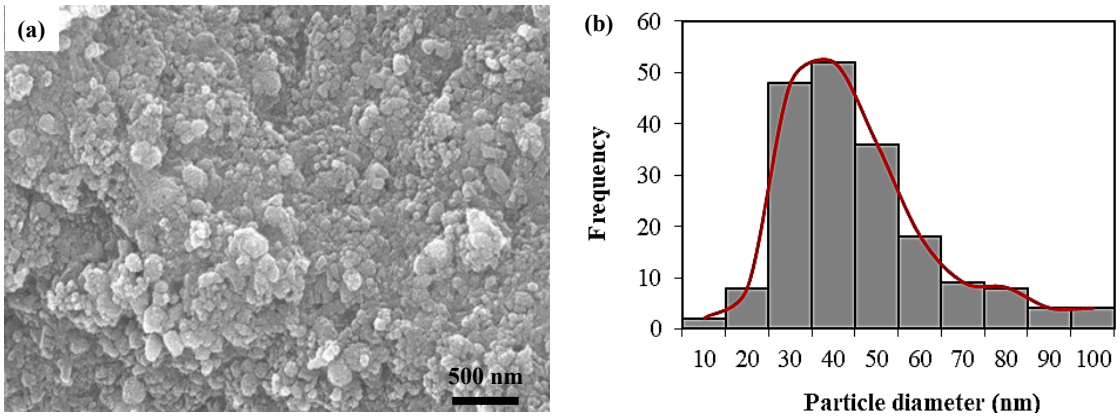


Figure 11. (a) SEM image, and (b) Particle size distribution of Ag NPs.

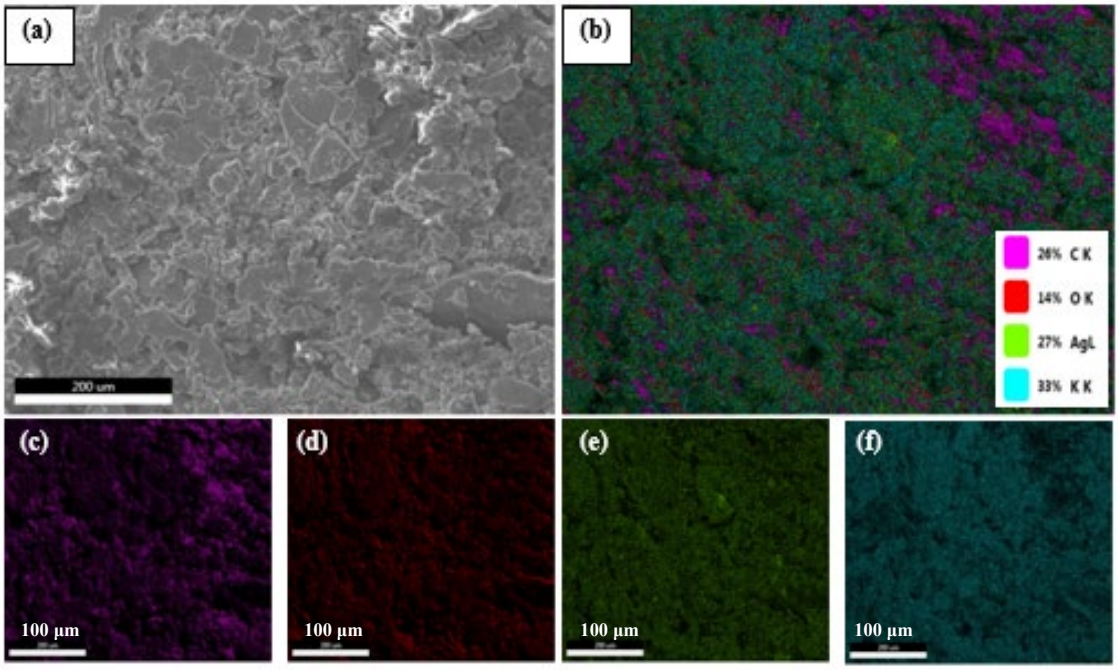


Figure 12. (a) SEM image of the area used for EDX mapping, (b) Elemental mapping of AgNPs with inset showing the weight percentages of the elements on the same spot: corresponding to, (c) carbon, (d) oxygen, (e) silver, and (f) potassium. Scale bar is 200 µm in (a), and 100 µm in (c–f).

Figure 12(a) showed the SEM image of the region where the EDX analysis was carried out. The corresponding elemental map in Figure 12(b) demonstrated that the major elements—carbon, oxygen, silver, and potassium—were uniformly distributed across the analyzed area. The inset confirmed that carbon and oxygen constituted a large portion of the detected elements, indicating the presence of plant-derived organic molecules coating the nanoparticle surfaces, which is typical for green-synthesized AgNPs. The individual elemental maps in Figure 12(c–f) further verified this distribution: carbon and oxygen appeared as continuous surface layers, while silver was observed as distinct yet evenly dispersed regions, confirming successful formation and localization of AgNPs. Potassium appeared at moderate levels, most likely originating from mineral components naturally present in the extract. As a consequence, the mapping results confirmed that the AgNPs contained a metallic Ag phase uniformly embedded within an organic-rich matrix derived from the aqueous plant extract.

The green-synthesized AgNPs were initially characterized through SEM, EDX, and XPS analyses in order to verify their successful formation and to elucidate their morphological and chemical features. These results confirmed that the nanoparticles were properly generated, exhibited the expected elemental composition, and possessed surface functional groups compatible with subsequent incorporation into the polymer matrix. After confirming the synthesis and properties of the AgNPs, AgNPs-embedded alginate films were prepared and examined using FTIR, XRD, SEM and EDX techniques. These analyses were conducted to evaluate the chemical interactions within the film structure, the incorporation and distribution of AgNPs, and the overall morphological and structural characteristics of the composite films.

FTIR analysis was conducted to identify the characteristic functional groups of the AgNPs@SA films and the related FT-IR spectra was presented in Figure 13(a). Accordingly, AgNPs@SA films had a broad band at 3339 cm^{-1}, which was attributed to O–H stretching vibrations of alginate hydroxyl groups and bound water, together with residual phenolic –OH groups originating from the plant extract used in the green synthesis. The bands at 1607 cm^{-1} and 1427 cm^{-1} corresponded

to the asymmetric and symmetric stretching modes of carboxylate (–COO^-) groups, characteristic of the guluronic and mannuronic units of alginate; slight shifts in these regions compared with the alginate reported in the literature were associated with coordination of –COO^- groups to metal nanoparticles. The peaks observed at 1318 cm^{-1}, 1088 cm^{-1} and 1032 cm^{-1} were assigned to C–O and C–O–C stretching vibrations within the polysaccharide backbone and glycosidic linkages, confirming that the alginate structure was preserved after AgNPs embedding. The band around 934 cm^{-1} was related to ring vibration modes of uronic residues in the alginate chain. As a result, these features indicated that the alginate matrix remained intact and that its hydroxyl and carboxylate groups participated in stabilizing the green-synthesized AgNPs within the film network, in agreement with reported AgNPs–alginate composite studies [45–47].

The XRD pattern presented in Figure 13(b) exhibited a broad peak at 12.5° (2θ), characteristic of the amorphous structure of the sodium alginate matrix. In addition to this amorphous profile, several diffraction peaks were observed at 38.10°, 45.51°, 66.29°, 75.32°, and 84.07° which aligned with the typical lattice planes of face-centered cubic (fcc) silver. These reflections were assigned to the (111), (200), (220), (311), and (222) planes, indicating that the AgNPs embedded within the alginate film maintained their crystalline structure. The presence of these characteristic fcc peaks confirmed the successful incorporation of crystalline AgNPs into the polymer network [45,48–50]. On the other hand, the additional peaks observed at 31.78° and 56.53° may be associated with residual crystalline organic constituents originating from the avocado peel extract [51–52].

The SEM images presented in Figure 14 showed the surface morphology of the AgNPs@SA films at different magnifications. At 10000x, the films exhibited an irregular and folded structure typical of dried alginate networks. Increasing the magnification to 20,000x revealed particulate aggregates within the examined regions of the polymer matrix. At the highest magnification (100 000x), these aggregates became more clearly defined, appearing along pore edges and within surface cavities of the alginate film. The overall morphology confirmed that the AgNPs were effectively incorporated into the alginate network and were retained as nanoscale aggregates rather than isolated particles.

The EDX analysis (Figure 15) showed that the films contained primarily chloride (50%) and calcium (24%), along with notable amounts of sodium (19%) and oxygen (4%), which was consistent with the composition of crosslinked alginate. The high Ca and Cl levels reflected the $CaCl_2$ crosslinking step, while residual Na^+ originated from the sodium alginate backbone. The oxygen and carbon signals corresponded to the polysaccharide matrix, and the small boron content likely derived from minor components of the plant extract. Silver was not detected in this mapping area, which can occur when its local concentration was low relative to the dominant alginate and crosslinking ions; however, the presence of AgNPs in the films was supported by XRD data.

The comprehensive characterization results provided valuable information on the structural and chemical properties of the developed AgNPs@SA films, supporting their further investigation as potential wound dressing materials.

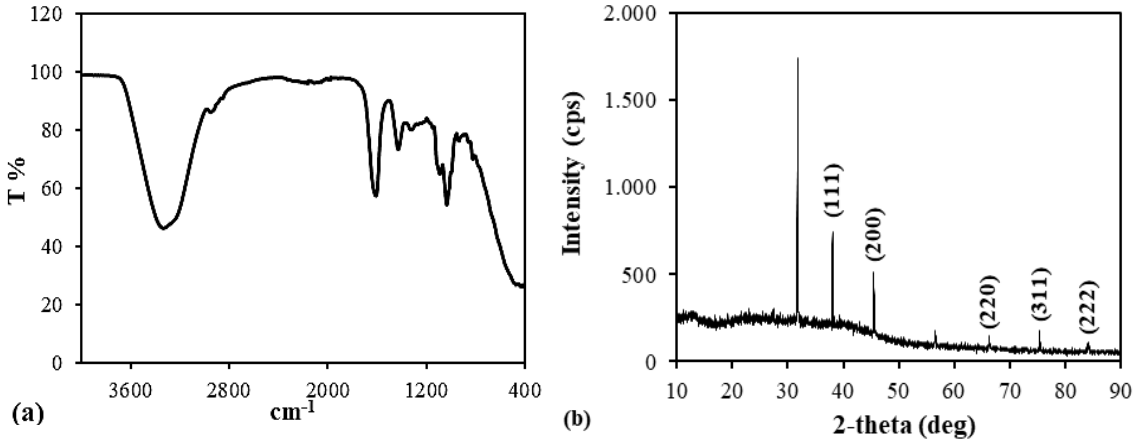


Figure 13. (a) FT-IR spectra, and (b) XRD pattern of AgNPs@SA films.

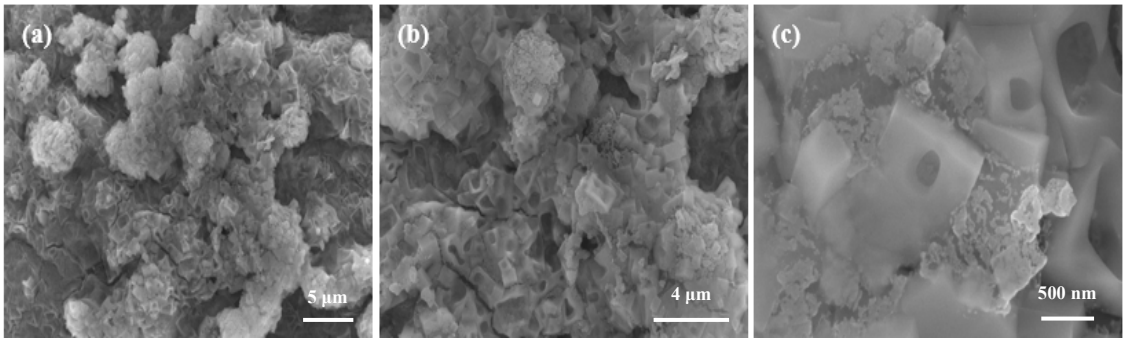


Figure 14. SEM images of AgNPs@SA films at different magnifications: (a) 10 000X, (b) 20 000X, and (c) 100 000X.

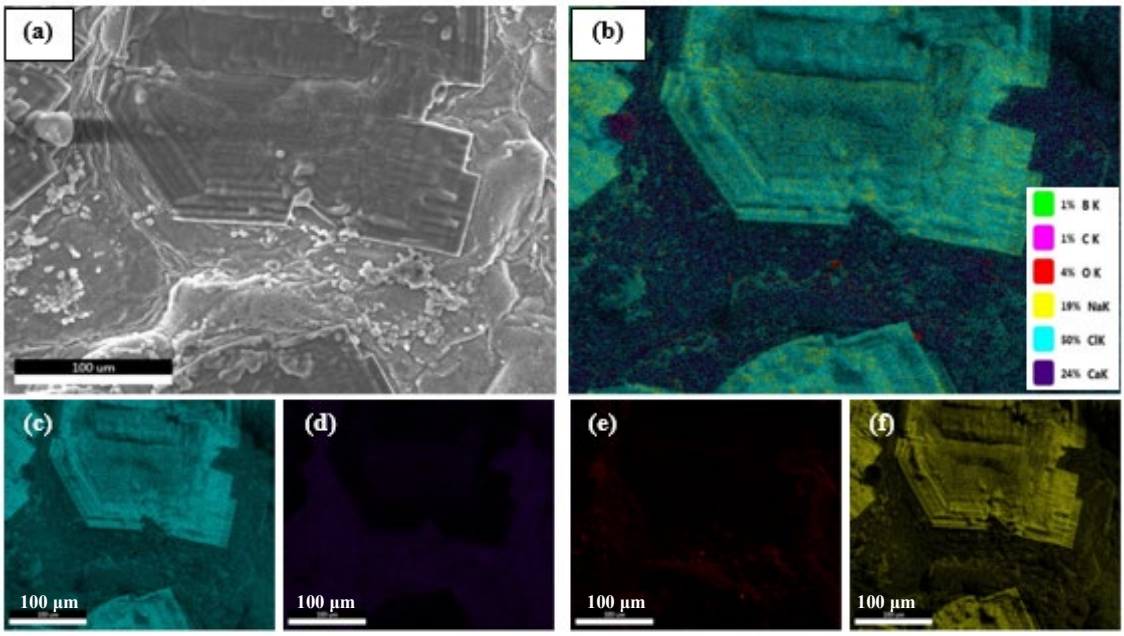


Figure 15. (a) SEM image of the area used for EDX mapping, (b) Elemental mapping of AgNPs@SA films with inset showing the weight percentages of the elements on the same spot: corresponding to (c) chlorine, (d) calcium, (e) oxygen, and (f) sodium.

3.3 Limitations and future perspectives

The developed AgNPs@SA films exhibited promising physico-chemical, mechanical, and antibacterial properties, providing a basis for further investigation of their potential as wound dressing materials. An important aspect requiring further consideration is the release behavior of silver from the polymer matrix. Silver release plays a significant role in the performance of silver-containing wound dressings, as the amount and rate of released silver species can influence both antimicrobial efficacy and cellular responses. Previous studies on silver-containing alginate films have highlighted the relationship between silver release characteristics and biological performance, emphasizing the importance of evaluating release behavior alongside antibacterial activity and cellular compatibility [22,32]. In the present study, the swelling behavior, water resistance, and weight loss of the films were systematically investigated, providing information on their interactions with aqueous environments and structural stability. Building upon these findings, future investigations should focus on the quantitative evaluation of time-dependent silver release under simulated wound conditions. The influence of the release medium should also be considered, as its ionic composition and protein content may affect silver dissolution, complexation, and bioavailability. Such investigations would provide further insight into the relationship between the physicochemical characteristics of the films, silver release behavior, and their potential biological performance.

Another important aspect for the further development of AgNPs @SA films is the evaluation of their cytocompatibility and hemocompatibility. The antibacterial activity observed against *Staphylococcus aureus* and *Pseudomonas aeruginosa* demonstrates the antimicrobial potential of the developed films. For wound dressing applications, however, the interaction of silver-containing materials with mammalian cells is also particularly important, since silver species may influence the viability, proliferation, and function of cells involved in tissue repair. Previous studies on silver-containing alginate composites have investigated cellular responses using fibroblasts and keratinocytes, highlighting the importance of considering both antibacterial performance and cellular compatibility during material development [22,32,53]. Accordingly, future studies should include in vitro cytocompatibility assessments using relevant fibroblast and keratinocyte cell lines. Both direct-contact and extract-based assays could provide complementary information on cellular responses to the films and their released components. The inclusion of appropriate control materials, such as silver-free alginate films, would also facilitate the evaluation of the contribution of silver-containing components to the observed biological effects. Furthermore, hemocompatibility assessments, including hemolysis testing where relevant to the intended application, would provide additional information on the interactions between the developed materials and blood components.

In addition to these evaluations, further investigation of the wound-healing potential of AgNPs@SA films would be valuable. Cellular processes such as fibroblast proliferation, keratinocyte migration, and tissue regeneration play essential roles in wound healing and represent important considerations in the development of functional wound dressing materials. Therefore, future studies could incorporate appropriate in vitro wound-healing models to evaluate cellular migration and proliferation in the presence of the developed films, followed by in vivo investigations to assess their performance under more complex physiological conditions. In conclusion, the physicochemical, mechanical, and antibacterial findings obtained in this study provide a foundation for the continued development of avocado peel-derived AgNPs@SA films as potential wound dressing candidates, while further investigations of silver release and biological compatibility will contribute to a more comprehensive evaluation of their application potential.

4. Conclusions

In this study, AgNPs were synthesized using the extract of waste avocado peels as reducing and stabilizing agents, and then embedded into alginate films. The prepared materials (AgNPs and AgNPs@SA film) were separately characterized, revealing that the average particle diameter of AgNPs was 49.8 nm, they had a face-centered cubic crystal structure, and that phytochemical components in the plant extract played a role in the synthesis of AgNPs. The XRD result provided supporting evidence for the presence of AgNPs within the alginate film. After structural verification through characterization, various physicochemical properties of AgNPs@SA films were investigated to evaluate their usability as wound dressings. The results showed that formulation parameters such as alginate amount, $AgNO_3$ concentration, and extract concentration significantly affected the physicochemical properties of the films. Accordingly; increasing alginate, $AgNO_3$, and extract concentrations led to the formation of denser and more cross-linked network structures; this resulted in increased water resistance and gel fraction, while allowing for the adjustment of swelling and degradation properties. Among the films tested, the film with a composition of 2.0 g alginate, 2.0 mM $AgNO_3$, and 0.20 $g{\cdot}mL^{-1}$ extract demonstrated the most desirable performance in terms of structural integrity, moisture management, and biodegradability.

The obtained optimum AgNPs@SA film exhibited suitable thickness, stable WVTR values, and notable antibacterial activity against *S. aureus* and *P. aeruginosa*, thus suggesting its potential as a candidate material for wound dressing applications. The mechanical findings indicated that the film is flexible and durable enough to maintain its structural integrity during application to wound surfaces and throughout use.

The results of this study highlight an environmentally friendly and efficient approach to converting avocado peel waste into high-value antimicrobial biomaterials. Although the obtained results are encouraging, the developed AgNPs@SA films should be regarded as preliminary candidates for potential wound dressing applications. Further investigations, particularly quantitative silver-release studies, cytocompatibility and hemocompatibility assessments, and cellular and in vivo wound-healing evaluations, are required to establish their biological safety and therapeutic potential.

Ethics approval

Not applicable.

Author contributions

Rasha Abdulbari: Investigation, Data curation.

Deniz Uzunoğlu Doğruyol: Conceptualization, Writing – original draft, Writing – review & editing, Methodology, Project administration, Software, Validation, Visualization.

Ayla Özer: Funding acquisition, Supervision, Resources.

Data availability

Data will be made available on request.

Acknowledgment

This work was supported by the Mersin University Scientific Research Projects Unit (Project No: 2025-TP2-5335).

Conflict of interest

The authors declare that they have no conflict of interest.

References

[1] G. Şahin, "One of the new actors of turkish agriculture: avocado (Persea americana Mill.)," *Journal of Anatolian Geography*, vol. 2, no. 2, pp. 70–83, 2024.

[2] A. Féliz-Jiménez, and R. Sanchez-Rosario, "Bioactive compounds, composition and potential applications of avocado agro-industrial residues: A review," *Applied Sciences (Switzerland)*, vol. 14, no. 21, p. 10070, 2024.

[3] M. A. Oke, E. A. Adebayo, N. A. Ajisope, B. M. Olowe, and O. S. Fasuan, "Avocado (Persea americana) peel: A promising source of bioactive compounds," *Frontiers in Nutrition,* vol. 12, no. october, p. 1642969, 2025,

[4] D. Merino, L. Bertolacci, U. C. Paul, R. Simonutti, and A. Athanassiou, "Avocado peels and seeds: Processing strategies for the development of highly antioxidant bioplastic films," *ACS Applied Materials & Interfaces*, vol. 13, no. 32, pp. 38688–38699, 2021.

[5] A. P. S. Nascimento, M. E. M. Duarte, A. P. T. Rocha, and A. N. Barros, "Valorization of avocado (Persea americana) peel and seed: Functional potential for food and health applications," *Antioxidants*, vol. 14, no. 9, pp. 1–20, 2025.

[6] F. Anjum, A. Saddiqa, M. M. Nazir, R. Naseer, M. Riaz, and A. Ashraf, "Avocado peel-derived polyphenols and date palm mucilage as natural macromolecules in the green synthesis of antimicrobial silver nanoparticles for wound dressing applications," *International Journal of Biological Macromolecules*, vol. 329, no. 1, Art. no. 147771, 2025.

[7] V. U. M. Nallal, K. Prabha, and M. Razia, "Avocado-waste mediated synthesis of silver nanoparticles and exploration of their potential biological properties," in *Materials Today: Proceedings*, Elsevier Ltd, Jan. 2022, pp. 1745–1749.

[8] N. Jayarambabu, A. Akshaykranth, T. Venkatappa Rao, K. Venkateswara Rao, and R. Rakesh Kumar, "Green synthesis of Cu nanoparticles using Curcuma longa extract and their application in antimicrobial activity," *Materials Letters*, vol. 259, Art. no. 126813, 2020.

[9] A. Estifanos, H. B. Abebe, and B. Gelagay, "Green Synthesis and analysis of Ni–Cu, Ni–Ag, and Cu–Ag bimetallic nanoparticles using avocado (Persea Americana) peel extract for sustainable antibacterial applications," *Journal of Nanotechnology*, vol. 2025, no. 1, Art. no. 8879390, 2025.

[10] S. A. Behera, A. Amanat, and P. G. R. Achary, "Photocatalytic degradation of ciprofloxacin drug utilizing novel PVDF/polyaniline/lanthanum strontium manganate@Ag composites," *Journal of Metals, Materials and Minerals*, vol. 34, no. 1, Art. no. 1896, 2024.

[11] E. Ali, S. H. Abu-Hussien, E. Hesham, S. Ahmed, H. Mostafa, A. Gamal, S. M. El-Sayed, B. Hemdan, A. Bakry, N. M. Ebeed, H. Elhariry, A. Galal, and B. T. Abd-Elhalim, "Compatibility and antimicrobial activity of silver nanoparticles synthesized using Lycopersicon esculentum peels," *AMB Express*, vol. 14, no. 1, Art. no. 124, 2024.

[12] A. S. Rodrigues, J. G. S. Batista, M. Á. V. Rodrigues, V. C. Thipe, L. A. R. Minarini, P. S. Lopes, and A. B. Lugão, "Advances in silver nanoparticles: A comprehensive review on their potential as antimicrobial agents and their mechanisms of action elucidated by proteomics," *Frontiers in Microbiology* vol. 15, p. 1440065, 2024.

[13] R. K. Kandikonda, R. Katru, N. Madathil, N. Venkatesh, R. Nagapuri, R. K. Rajaboina, H. Divi, C. R. Mallu, M. Dhayalan, G. Murugadoss, and K. U. Kumar, "Metal-displacement-derived silver nanoparticles for visible-light catalysis and TENG-enabled circuit integration," *Scientific Reports*, vol. 16, no. 1, Art. no. 14780, 2026.

[14] A. Subhadarshini, E. Subudhi, P. G. R. Achary, S. A. Behera, N. Parwin, and B. Nanda, "ZIF-8 supported Ag_3PO_4/g-C_3N_4 a Double Z-scheme heterojunction: An efficient photocatalytic, antibacterial and hemolytic nanomaterial," *Journal of Water Process Engineering*, vol. 65, Art. no. 105901, 2024.

[15] N. Kučuk, M. Primožič, Ž. Knez, and M. Leitgeb, "Sustainable biodegradable biopolymer-based nanoparticles for healthcare applications," *International Journal of Molecular Sciences*, vol. 24, no. 4, p. 3188, 2023.

[16] R. Abka-khajouei, L. Tounsi, N. Shahabi, A. K. Patel, S. Abdelkafi, and P. Michaud, "Structures, properties and applications of alginates," *Marine Drugs*, vol. 20, no. 364, pp. 1–18, 2022.

[17] I. P. S. Fernando, W. W. Lee, E. J. Han, and G. Ahn, "Alginate-based nanomaterials: Fabrication techniques, properties, and applications," *Chemical Engineering Journal*, vol. 391, no. July 2019, p. 123823, 2020.

[18] Y. Wang, Q. Li, X. Peng, Z. Li, J. Xiang, Y. Chen, K. Hao, S. Wang, D. Nie, Y. Cui, F. Lv, Y. Wang, W. Wu, D, Guo, and H. Si, "Green synthesis of silver nanoparticles through oil: Promoting full-thickness cutaneous wound healing in methicillin-resistant *Staphylococcus aureus* infections," *Frontiers in Bioengineering and Biotechnology*, vol. 10, no. August, pp. 1–19, 2022.

[19] A. Gudimalla, J. Jose, J. V. Rajendran, G. Gurram, and S. Thomas, "Synthesis of silver nanoparticles by plant extract, incorporated into alginate films and their characterizations," *Chemical Papers*, vol. 76, no. 2, pp. 1031–1043, 2022.

[20] D. P. da Silva, A. d. S. Silva, J. V. M. da Silva, L. M. de Melo Silva, J. J. da Silva Neto, I. F. Moreira, R.Moreira, and A. C. A. Silva, "Emerging trends in wound management using alginate- based dressings functionalized with metallic nanoparticles : A scoping review," *Journal of Exploratory Research in Pharmacology*, vol. 10, no. 4, p. e00029, 2025.

[21] A. Barbu, B. Neamtu, M. Zăhan, G. M. Iancu, C. Bacila, and V. Mireșan, "Current trends in advanced alginate-based wound dressings for chronic wounds," *Journal of Personalized Medicine,* vol. 11, no. 9, p. 890, 2021.

[22] V. Ambrogi, D. Pietrella, A. Donnadio, L. Latterini, A. D. Michele, I. Luffarelli, and M. Ricci, "Biocompatible alginate silica supported silver nanoparticles composite films for wound dressing with antibiofilm activity," *Materials Science and Engineering C*, vol. 112, p. 110863, 2020.

[23] M. Alloisio, A. Dodero, S. Alberti, S. Vicini, and M. Castellano, "Electrospun alginate mats embedding silver nanoparticles with bioactive properties," *International Journal of Biological Macromolecules*, vol. 213, pp. 427–434, 2022.

[24] F. R. Diniz, R. C. A. P Maia, L. Rannier, L. N. Andrade, M. V. Chaud, C. F. da Silva, C. B. Corrêa, R. L. C. de Albuquerque Junior, L. P. da Costa, S. R. Shin, S. Hassan, E. Sanchez-Lopez, E. B. Souto, and P Severino, "Silver nanoparticles-composing alginate/gelatine hydrogel improves wound healing in vivo," *Nanomaterials*, vol. 10, no. 2, p. 390, 2020.

[25] A. Froelich, E. Jakubowska, M. Wojtyłko, B. Jadach, M. Gackowski, P. Gadziński, O. Napierała, Y. Ravliv, and T. Osmałek, "Alginate-based materials loaded with nanoparticles in wound healing," *Pharmaceutics*, vol. 15, no. 4, p. 1142, 2023.

[26] I. Panda, and S. A. Behera, "Multifunctional polyvinyl alcohol/ ionic liquid/silver composite for biomedical and electrical applications," *Polymer Bulletin*, vol. 82, no. 15, pp. 10051–10073, 2025.

[27] M. Ansari, S.Ahmed, A. Abbasi, M. T. Khan, M. Subhan, N. A. Bukhari, A. A. Hatamleh, and N. R. Abdelsalam, "Plant mediated fabrication of silver nanoparticles, process optimization, and impact on tomato plant," *Scientific Reports*, vol. 13, no. 1, pp. 1–19, 2023.

[28] L. Motelica, D. Ficai, O.-C. Oprea, A. Ficai, V.-L. Ene, B.-S. Vasile, E. Andronescu, and A.-M. Holban, "Antibacterial biodegradable films based on alginate with silver nanoparticles and lemongrass essential oil–innovative packaging for cheese," *Nanomaterials*, vol. 11, no. 9, p. 2377, 2021.

[29] R. Abdulbari, D. Uzunoğlu Doğruyol, and A. Özer, "Preparation and identification of alginate wound dressing/ biofilm loaded with silver nanoparticles biosynthesized from Avocado (Persea Americana) waste," in 9th *International Ankara Multidisciplinary Studies Congress*," 2025, pp. 338–375.

[30] M. M. Delavari, and I. Stiharu, "Preparing and Characterizing novel biodegradable starch/PVA-based films with nano-sized zinc-oxide particles for wound-dressing applications," *Applied Sciences (Switzerland)*, vol. 12, no. 8, p. 4001, 2022.

[31] J. Gubitosa, V. Rizzi, C. Marasciulo, F. Maggi, G. Caprioli, A. M. Mustafa, P. Fini, N. De Vietro, A. M. Aresta, and P. Cosma, "Realizing eco-friendly water-resistant sodium-alginate-based films blended with a polyphenolic aqueous extract from grape pomace waste for potential food packaging applications," *International Journal of Molecular Sciences*, vol. 24, no. 14, p. 11462, 2023.

[32] M. Puccetti, A. Donnadio, M. Ricci, L. Latterini, G. Quaglia, D. Pietrella, A. Di Michele, and V. Ambrogi, "Alginate Ag/AgCl nanoparticles composite films for wound dressings with anti-biofilm and antimicrobial activities," *Journal of Functional Biomaterials,* vol. 14, no. 2, p. 84, 2023.

[33] S. A. Asiri, A. Matar, A. M. Ismail, and H. A. S. Farag, "Sodium alginate edible films incorporating cactus pear extract: Anti-microbial, chemical, and mechanical properties," *Italian Journal of Food Science*, vol. 36, no. 4, pp. 151–168, 2024.

[34] B. Deepa, E. Abraham, L. A. Pothan, N. Cordeiro, M. Faria, and S. Thomas, "Biodegradable nanocomposite films based on sodium alginate and cellulose nanofibrils," *Materials*, vol. 9, no. 1, pp. 1–11, 2016.

[35] M. Moura-Alves, V. G. L. Souza, J. A. Silva, A. Esteves, L. M. Pastrana, C. Saraiva, and M. A. Cerqueira, "Characterization of sodium alginate-based films blended with olive leaf and laurel leaf extracts obtained by ultrasound-assisted technology," *Foods*, vol. 12, no. 22, p. 4076, 2023.

[36] J. H. Lee, D. Jeong, and P. Kanmani, "Study on physical and mechanical properties of the biopolymer/silver based active nanocomposite films with antimicrobial activity," *Carbohydrate Polymers*, vol. 224, no. August, p. 115159, 2019.

[37] L. M. Júnior, E. Jamróz, S. de Á. Gonçalves, R. G. da Silva, R. M. V. Alves, and R. P. Vieira, "Preparation and characterization of sodium alginate films with propolis extract and nano-SiO_2," *Food Hydrocolloids for Health*, vol. 2, no. September, p. 100094, 2022,

[38] K. Kanjanamekanant, T. Thanyacharoen, S. Techasakul, and P. Chuysinuan, "Fabrication of a cellulose-based wound dressing membrane from sugarcane bagasse biowaste," *ACS Omega*, vol. 10, no. 39, pp. 45232–45240, 2025.

[39] B. Chen, B. He, A. M. Tucker, I. Biluck, T. H. Leung, T. P. Schaer, and S. Yang, "An Environmentally stable, biocompatible, and multilayered wound dressing film with reversible and strong adhesion," *Advanced Healthcare Materials*, vol. 13, no. 31, pp. 1–15, 2024.

[40] K. Y. Lee, and D. J. Mooney, "Alginate: Properties and biomedical applications," *Progress in Polymer Science (Oxford)*, vol. 37, no. 1, pp. 106–126, 2012.

[41] Y. M. S. Jamil, A. N. Al-Hakimi, H. M. A. Al-Maydama, G. Y. Almahwiti, A. Qasem, and S. M. Saleh, "Optimum green synthesis, characterization, and antibacterial activity of silver nanoparticles prepared from an extract of aloe fleurentinorum," *International Journal of Chemical Engineering*, vol. 2024, no. 1, p. 2804165, 2024.

[42] H. Basalius, A. Mani, A. Michael, S. M. Mary, M. Lenin, P. Chelliah, M. R. Siddiqui, S. M. Wabaidur, and A. Islam, "Green synthesis of nano-silver using Syzygium samarangense flower extract for multifaceted applications in biomedical and photocatalytic degradation of methylene blue," *Applied Nanoscience (Switzerland)*, vol. 13, no. 6, pp. 3735–3747, 2023.

[43] B. O. Aljohny, A. A. A. Almaliki, Y. Anwar, M. Ul-Islam, and T. Kamal, "Antibacterial and catalytic performance of green synthesized silver nanoparticles embedded in crosslinked PVA sheet," *Journal of Polymers and the Environment*, vol. 29, no. 10, pp. 3252–3262, 2021.

[44] V. P. Manjamadha and K. Muthukumar, "Ultrasound assisted green synthesis of silver nanoparticles using weed plant," *Bioprocess and Biosystems Engineering*, vol. 39, no. 3, pp. 401–411, 2016.

[45] Y. Shao, C. Wu, T. Wu, C. Yuan, S. Chen, T. Ding, X. Ye, and Y. Hu, "Green synthesis of sodium alginate-silver nanoparticles and their antibacterial activity," *International Journal of Biological Macromolecules*, vol. 111, pp. 1281–1292, 2018.

[46] E. Susilowati, L. Mahardiani, and R. D. Hardini, "The effect of silver nanoparticles toward properties and antibacterial activity of silver-alginate nanocomposite films," *Frontiers in Sustainable Food Systems*, vol. 6, p. 1340-1341, 2022.

[47] S. Iswarya, N. Hariram, T. Theivasanthi, and S. C. B. Gopinath, "Green synthesis and formation of sodium alginate/silver nanocomposite as electroconductive films with enhanced antibacterial effects for biomedical applications," *Colloid and Polymer Science*, vol. 303, no. 12, pp. 2543–2557, 2025.

[48] K. Ramachandraiah, N. T. B. Gnoc, and K. B. Chin, "Biosynthesis of silver nanoparticles from persimmon byproducts and incorporation in biodegradable sodium alginate thin film," *Journal of Food Science*, vol. 82, no. 10, pp. 2329–2336, 2017.

[49] M. Amutha, P. Lalitha, and M. J. Firdhouse, "Biosynthesis of silver nanoparticles using Kedrostis foetidissima (Jacq.) Cogn," *Journal of Nanotechnology*, vol. 2014, no. 1, p. 860875, 2014,

[50] G. Marslin, R. K. Selvakesavan, G. Franklin, B. Sarmento, and A. C. P. Dias, "Antimicrobial activity of cream incorporated with silver nanoparticles biosynthesized from Withania somnifera," *International Journal of Nanomedicine*, vol. 10, pp. 5955–5963, 2015.

[51] S. Jain, and M. S. Mehata, "Medicinal plant leaf extract and pure flavonoid mediated green synthesis of silver nanoparticles and their enhanced antibacterial property," *Scientific Reports*, vol. 7, no. 1, Art. no. 15867, 2017.

[52] V. U. M. Nallal, K. Prabha, I. VethaPotheher, B. Ravindran, A. Baazeem, S. W. Chang, G. A. Otunola, and M. Razia, "Sunlight-driven rapid and facile synthesis of silver nanoparticles using Allium ampeloprasum extract with enhanced antioxidant and antifungal activity," *Saudi Journal of Biological Sciences*, vol. 28, no. 7, pp. 3660–3668, 2021.

[53] N. Kahya, A. Kartun, I. N. Korkut, C. Usta, D. S. Kuruca, and A. Gürarslan, "Silver nanowire-coated porous alginate films for wound dressing applications: Antibacterial Activity, cell proliferation, and physical characterization," *ACS Omega*, vol. 9, no. 50, pp. 49032–49042, 2024.